Published OnlineFirst June 29, 2015; DOI: 10.1158/0008-5472.CAN-14-3265

Tumor and Stem Cell Biology

Cancer Research

Diverse Targets of β-Catenin during the Epithelial–Mesenchymal Transition Define Cancer Stem Cells and Predict Disease Relapse

Yi-Wen Chang[1], Ying-Jhen Su[1], Michael Hsiao[2], Kuo-Chen Wei[3], Wei-Hsin Lin[1,4], Chi-Jung Liang[1], Shin-Cheh Chen[5], and Jia-Lin Lee[1,6]

Abstract

Wnt signaling contributes to the reprogramming and maintenance of cancer stem cell (CSC) states that are activated by epithelial–mesenchymal transition (EMT). However, the mechanistic relationship between EMT and the Wnt pathway in CSC is not entirely clear. Chromatin immunoprecipitation with high-throughput sequencing (ChIP-seq) indicated that EMT induces a switch from the β-catenin/E-cadherin/Sox15 complex to the β-catenin/Twist1/TCF4 complex, the latter of which then binds to CSC-related gene promoters. Tandem coimmunoprecipitation and re-ChIP experiments with epithelial-type cells further revealed that Sox15 associates with the β-catenin/E-cadherin complex, which then binds to the proximal promoter region of *CASP3*. Through this mechanism, Twist1 cleavage is triggered to regulate a β-catenin–elicited promotion of the CSC phenotype. During EMT, we documented that Twist1 binding to β-catenin enhanced the transcriptional activity of the β-catenin/TCF4 complex, including by binding to the proximal promoter region of *ABCG2*, a CSC marker. In terms of clinical application, our definition of a five-gene CSC signature (nuclear β-catenin^{High}/nuclear Twist1^{High}/E-cadherin^{Low}/Sox15^{Low}/CD133^{High}) may provide a useful prognostic marker for human lung cancer. *Cancer Res; 75(16); 3398–410. ©2015 AACR.*

Introduction

Tumor recurrence is one of the biggest challenges in cancer. The existence of cancer stem cells (CSC) may account for chemotherapeutic drug resistance and tumor recurrence. Mani and colleagues found that induction of epithelial–mesenchymal transition (EMT) also generates cells with stem cell–like properties (1). In addition, studies suggest that Wnt signaling contributes to the induction and maintenance of CSC states activated by the EMT program (2). The mechanistic relationship between EMT and the Wnt pathway in CSCs is thus a crucial issue.

EMT plays an essential role in the development of the mesoderm from the epithelium during embryogenesis. In addition to being a physiologic mechanism for development, EMT is also recognized as a pathologic mechanism in the progression of various diseases, including inflammation, fibrosis, and cancer (3). During EMT, cells undergo dramatic phenotypic changes as epithelial cell types are converted into cells with mesenchymal attributes, and they become motile and invade the extracellular matrix (3). EMT induction in tumor cells upon treatment with TGFβ or overexpression of the key EMT inducers Snail and Twist results in an increased ability of cells to form tumorspheres and to express CSC markers (1). Moreover, Twist1 induces the expression of the stemness gene *Bmi1* to promote EMT and the tumor-initiating capability of head and neck cancer cells (4). Together, this diverse evidence suggests that inducers of EMT may be involved in reprogramming differentiated tumor cells into CSCs. However, the molecular mechanism for the initiation and maintenance of these stem cell–like traits remains unclear.

In this study, we found that EMT induction is not sufficient to generate cells with properties of CSCs. Our results indicate that autocrine/paracrine signaling might play a key role in maintaining the mesenchymal state and subsequent promotion of the CSC phenotype. These findings illuminate a direct link between the microenvironment niche and EMT in promotion of the CSC phenotype, which may be beneficial in designing effective cancer therapeutics.

Materials and Methods

Cell lines

All cell lines were obtained from the ATCC. They were tested and authenticated by short tandem repeat analysis (in 2015).

Constructs and reagents

The DKK1 expression construct was obtained from Addgene. The SFRP1 expression construct (5) was a gift from Ya-Wen Lin (National Defense Medical Center, Taipei, Taiwan). The Twist1 expression construct (6) was a gift from Kimitoshi Kohno

[1]Institute of Molecular and Cellular Biology, National Tsing Hua University, Hsinchu, Taiwan. [2]Genomics Research Center, Academia Sinica, Nankang, Taipei, Taiwan. [3]Department of Neurosurgery, Chang-Gung Memorial Hospital, Linkou, Taiwan. [4]Department of Orthopedics, National Taiwan University Hospital Hsin-Chu Branch, Hsinchu, Taiwan. [5]Department of Surgery, Chang-Gung Memorial Hospital, Linkou, Taiwan. [6]Department of Medical Science, National Tsing Hua University, Hsinchu, Taiwan.

Note: Supplementary data for this article are available at Cancer Research Online (http://cancerres.aacrjournals.org/).

Y.-W. Chang and Y.-J. Su contributed equally to this article.

Corresponding Author: Jia-Lin Lee, Institute of Molecular and Cellular Biology, National Tsing Hua University, 101, Section 2, Kuang-Fu Road, Hsinchu 30013, Taiwan. Phone: 886-3-5742002; Fax: 886-3-5715934; E-mail: jllee@life.nthu.edu.tw

doi: 10.1158/0008-5472.CAN-14-3265

Published OnlineFirst June 29, 2015; DOI: 10.1158/0008-5472.CAN-14-3265

(University of Occupational and Environmental Health, Kitakyushu, Japan). Twist1 mutants with a C-terminal deletion (ΔC; residues 184–202 deleted) and an N-terminal deletion (ΔN; residues 1–111 deleted) were generated by PCR amplification of the corresponding cDNA fragments using wild-type Twist1 as a template. The Twist1 mutant (Twist1D169A) (7) was generated by site-directed mutagenesis using the wild-type Twist1 as a template. The correct sequence of the clones was verified by sequencing. Plasmid pLKO.1-shRNA encoding an shRNA with a scrambled sequence or sequences targeting human Sox15 and E-cadherin (National RNAi Core Facility) was introduced into HEK293T cells using the lentiviral packaging vectors pMD.G and pCMV_8.91. Antibodies against the following proteins were used: E-cadherin (610181; BD Biosciences); Twist1 (Ab50887), histone H3 (Ab1791), and ABCG2 (Ab3380; all from Abcam); active β-catenin (ALX-804-260/1; dephosphorylated at Ser33/37; Enzo Life Sciences); total β-catenin (C2206), β-actin (A5441), and TCF4 (T5817; all from Sigma); and phospho-β-catenin (phosphorylated at Ser33/37/Thr41; 9561; Cell Signaling Technology).

Microarray data collection and analysis

Total cellular RNA was extracted from LM and HM20 cells after treatment with or without Wnt3a. Approximately 2 mg of RNA was labeled and hybridized to Human HT-12 arrays (Illumina). Expression values were determined with GenomeStudio Data Analysis Software (Illumina), and this software was used for all data analysis. The data discussed in this publication have been deposited in National Center for Biotechnology Information Gene Expression Omnibus (GEO, http://www.ncbi.nlm.nih.gov/geo/) and are accessible through GEO Series accession number GSE67571.

Human samples and immunohistochemical analysis

Sectioned human lung cancer specimens were obtained from GenDiscovery Biotechnology, Inc. All staining procedures were performed using a Super Sensitive IHC Detection Systems kit (BioGenex). Counterstaining was performed with hematoxylin. A semiquantitative method for calculating positive signals was used. Signals were counted in 6 fields per sample under a light microscope at ×400 magnification. The results were manually evaluated by 2 independent observers to determine both the percentage of positive cells and the staining intensity, as previously described (8). The observers were blinded to the stage of each sample. The IHC score was obtained by multiplying the staining intensity (0, no expression; 1, weak expression; 2, moderate expression; 3, strong expression; and 4, very strong expression) by the percentage of positive cells (0, 0%–5% expression; 1, 6%–25% expression; 2, 26%–50% expression; 3, 51%–75% expression; and 4, 76%–100% expression) in the field. The maximum possible IHC score was $4 \times 4 = 16$.

Chromatin immunoprecipitation with high-throughput sequencing

Chromatin immunoprecipitation with high-throughput sequencing (ChIP-seq) experiments and data processing were performed as described previously (9). For β-catenin ChIP, we chemically crosslinked and sonicated cells to generate fractionated gDNA. The DNA was immunoprecipitated with anti-β-catenin (Sigma). The DNA fragments were blunt-end ligated to the Illumina adaptors, amplified, and sequenced (IlluminaHiSeq 2000). All reads were mapped to the Human Reference genome build 37 (hg19) using Burrows–Wheeler Alignment (10), and only uniquely matched reads were retained. A parallel version of MEME (Multiple EM for Motif Elicitation; ref. 11) software was used to perform a *de novo* search of consensus binding motifs for β-catenin. The peak sequences were annotated using the tool MEME-ChIP (12, 13) search against the JASPAR CORE 2009 vertebrates (14) databases and UniPROBE database (15). Given a set of human genomic regions, this tool performs (i) *ab initio* motif discovery, (ii) motif enrichment analysis, (iii) motif visualization, (iv) binding affinity analysis, and (v) motif identification.

ChIP and re-ChIP assays

The ChIP-seq assays were performed as described previously (16). For re-ChIP assays, immunoprecipitates were sequentially washed. Complexes were eluted by incubation with 10 mmol/L dithiothreitol (DTT) at 37°C for 30 minutes, diluted 50 times with dilution buffer (17), and then followed by a second immunoprecipitation with the indicated antibodies. Extracted DNA was analyzed by PCR using primers spanning the proximal promoter regions of *CDH1* (nucleotide positions −276/−95), *ABCG2* (−1250/−1050), or *CASP3* (−456/−276). Following 30 cycles of amplification, PCR products were run on a 1.5% agarose gel and analyzed by ethidium bromide staining.

Western blotting

Western blotting was performed as described previously (18).

Sphere-forming culture and self-renewal capability assays

Spheres were generated as described previously (9). Briefly, cells were grown in suspension culture using ultra-low attachment plates (Corning) and serum-free RPMI (Gibco) supplemented with B27 (Invitrogen), 20 ng/mL EGF, and 10 ng/mL basic fibroblast growth factor (bFGF; BD Biosciences). Spheres with a diameter of >30 μm were then counted. For serial passages (the self-renewal capability assays), spheres were harvested and dissociated to single cells with trypsin, and dissociated cells were replated in a 96-well plate (diluted to 1 cell per well in an ultra-low attachment plate) and cultured for 12 days. The spheres were then counted again. The individual spheres were found to be derived from single cells (1).

Identification and isolation of side population cells

Side population cells were identified as described previously (9).

Animal experiments

Severe combined immunodeficient (SCID) CB17 female mice (6 weeks old) were used, and all experiments were carried out with the approval of the local regulatory authorities. For the *in vivo* tumorigenicity assay, mice were injected subcutaneously with 10^2 to 10^4 cells in 100 μL of a 1:1 mixture of DMEM (with or without Wnt3a)/Matrigel. Tumorigenicity was evaluated at 4 weeks after transplantation.

Statistical analysis

Statistical analysis of data was performed with the Student *t* test using SigmaPlot software. The Fisher exact test was used for comparisons between groups. Differences were considered to be statistically significant at $P < 0.05$.

Published OnlineFirst June 29, 2015; DOI: 10.1158/0008-5472.CAN-14-3265

Results

EMT induction is not sufficient to generate cells with properties of CSCs

A recent report has suggested that there may be a direct link between EMT and the acquisition of CSC properties (1). Diverse extracellular signals have been reported to induce EMT in various cell types. To determine whether cancer cells that have undergone EMT and CSCs have similar traits, we induced EMT in serially selected cells (LM and HM1-HM20 cells as described in Supplementary Fig. S1 and Supplementary Information) by exposure to extracellular ligands, including TGFβ (19), Wnt3a (20), Wnt5a (21), and BMP4 (Fig. 1A–C; ref. 22). Interestingly, TGFβ was capable of reducing E-cadherin expression (Fig. 1A and Supplementary Fig. S2) but did not promote the CSC phenotype that possesses increased ability to form spheres in culture over 4 serial passages (Fig. 1B) or side population cells (Fig. 1C and Supplementary Fig. S3). In contrast, Wnt3a was incapable of reducing E-cadherin expression relative to untreated cells (Fig. 1A) but promoted the CSC phenotype in cells expressing lower E-cadherin levels with higher efficiency than other EMT inducers (Fig. 1B and C).

To substantiate the results described above, we performed a 48,804-feature microarray analysis on the expression profiles of LM and HM20 cells after treatment with or without Wnt3a. Because HM20 cells already exhibited an EMT phenotype (Fig. 1D), we wanted to determine whether this phenotype was associated with CSC properties. Prior to treatment with Wnt3a, we did indeed find genes in categories including self-renewal markers (Fig. 1E), CSC markers (Fig. 1F), and ATP-binding cassette (ABC) transporter genes (Fig. 1G), which were only slightly upregulated in HM20 cells relative to LM cells. These data again show that EMT induction is not sufficient to generate cells with properties of CSCs, indicating that regulation of the CSC phenotype requires additional elements. More importantly, after treatment with Wnt3a, many CSC-related genes were substantially upregulated in HM20 cells, whereas they were not upregulated in LM cells (Fig. 1E–G).

Transcription cofactor β-catenin has diverse targets in cells undergoing EMT upon stimulation with Wnt3a

To substantiate the results (Fig. 1E–G) showing differences in the expression profiles of LM and HM20 cells after treatment with Wnt3a, we performed ChIP-seq analysis to identify the genome-wide distribution of genes bound by the β-catenin complex in LM and HM20 cells after stimulation with Wnt3a. We investigated whether the β-catenin transcription cofactor bound to different gene loci and motifs in LM and HM20 cells. Details of the number of reads that underwent data preprocessing are presented in Supplementary Tables S1 (LM cells, top) and S2 (HM20 cells, top). We identified multiple peaks across the selected chromosomes in LM (red, top) and HM20 (green, bottom) cells (Fig. 2A). Most genome sequences bound by the β-catenin complex in LM and HM20 cells were distinct. The 30 highest scoring (Tag number) genes selected are shown in Supplementary Tables S1 (LM cells, bottom) and S2 (HM20 cells, bottom).

Next, we evaluated localized β-catenin–dependent transcriptional regulation of β-catenin-occupied genes that contribute to the properties of CSCs. Some of the ABC transporter genes are well-known to be regulated by β-catenin (23). As shown in Fig. 2B, we identified multiple peaks across the extended locus of the selected ABC transporter genes in HM20 cells (green, bottom) but not in LM cells (red, top).

We examined the comparative distribution of β-catenin–binding sites in LM and HM20 cells and found that 17.6% (964 of 5,490) of β-catenin–occupied sites in LM cells and 19.4% (5,520 of 28,421) of β-catenin–occupied sites in HM20 cells were located in promoters (Fig. 2C). Notably, 38.5% (2,113 of 5,490) of β-catenin–binding sites in LM cells and 32.8% (9,332 of 28,421) of β-catenin–binding sites in HM20 cells were localized to intergenic regions, where they could potentially function as distal enhancers or promoters of unannotated transcripts (Fig. 2C). To enumerate β-catenin–bound genes in LM and HM20 cells, we identified 675 and 7,095 genes uniquely bound by β-catenin in LM and HM cells, respectively. Interestingly, 1,667 genes were bound by β-catenin in both cell types (Fig. 2D). TCF-binding elements have been found in the promoter regions of many TCF target genes and are characterized by a highly conserved consensus sequence, 5′-CTTTG(A/T)(A/T)-3′ (24). The number of β-catenin/TCF complexes bound to the conserved motifs after Wnt3a treatment was dramatically greater in HM20 cells than in LM cells (Fig. 2E).

To determine whether other elements were identifiable in our genome-wide analysis, we carried out *de novo* searches of consensus motifs of β-catenin–bound regions in LM and HM20 cells using MEME software (Fig. 2F; refs. 12, 13). We further validated these results with side population percentage assays after the elimination of transcription factor transcripts by RNA interference (RNAi). Sox15 in LM cells was a negative regulator (Supplementary Fig. S4A), and TCF4 in HM20 cells was required for promotion of the CSC phenotype that was elicited by Wnt/β-catenin (Supplementary Fig. S4B). Thus, β-catenin plays discrete roles in epithelial and mesenchymal cells after stimulation with Wnt3a.

EMT acts as a molecular switch from β-catenin/E-cadherin/Sox15 to β-catenin/Twist1/TCF4 complex formation

To substantiate the results of ChIP-seq analysis, we performed tandem coimmunoprecipitation (Fig. 3A–C; ref. 16) and re-ChIP (Fig. 3D) experiments. In LM cells, Sox15 in complex with β-catenin and E-cadherin (Fig. 3A) bound to the proximal promoter region of *CASP3* (Fig. 3D) in a manner that was enhanced by Wnt3a stimulation. In HM20 cells, Twist1 in complex with β-catenin and TCF4 (Fig. 3B) bound to the proximal promoter region of *ABCG2* (Fig. 3D) after Wnt3a stimulation. These data indicate that EMT (in this case a transition from LM to HM20 cells) induces a switch from the formation of β-catenin/E-cadherin/Sox15 complexes to the formation of β-catenin/Twist1/TCF4 complexes, which then bind to related gene promoters (a switch from *CASP3* to *ABCG2* promoters, for example). Similar results were shown previously in CL1-0 (epithelial-type) and CL1-5 (mesenchymal-type) cells (Supplementary Fig. S5; ref. 25). Taken together, these results indicate that the transcription cofactor β-catenin binds to diverse targets in cells undergoing EMT upon stimulation with Wnt3a.

β-Catenin/E-cadherin/Sox15 and β-catenin/Twist1/TCF4 possess opposing effects in regulating Wnt-elicited promotion of the CSC phenotype

Using the cells that were serially selected for invasiveness (as shown in Supplementary Fig. S1), we found that Wnt3a, but not Twist1, increased TOPflash (a reporter plasmid containing

Published OnlineFirst June 29, 2015; DOI: 10.1158/0008-5472.CAN-14-3265

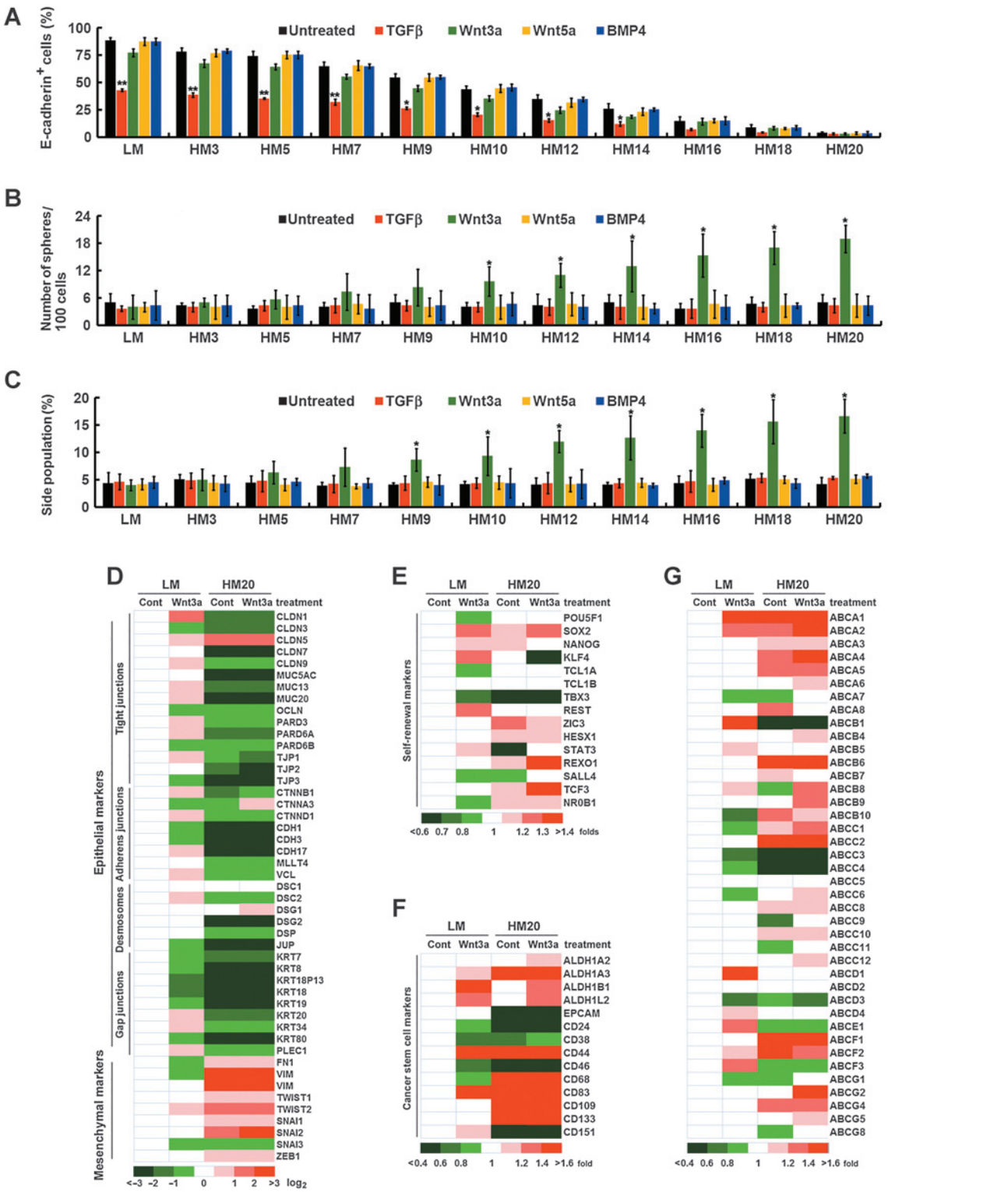

Figure 1.

EMT followed by canonical Wnt signaling stimulation generates cells with properties of CSCs. A, cells were exposed to extracellular ligands (TGFβ, Wnt3a, Wnt5a, and BMP4). The percentage of E-cadherin expression was determined by flow cytometry. B, *in vitro* quantification of spheres formed by cells over four serial passages. The individual spheres were found to be derived from single cells. C, cells were stained with Hoechst 33342, and side population (SP) cells were counted. D–G, 48804-feature microarray analysis was performed on the expression profiles of LM and HM20 cells after treatment with control medium (Cont) or Wnt3a-containing medium. The genes clustered were grouped into five categories on the basis of their cellular functions and properties. These categories included epithelial/mesenchymal marker genes (D), self-renewal marker genes (E), CSC marker genes (F), and the ABC transporter family genes (G). Representative clusters of the indicated genes are shown as heatmaps, with red indicating increased expression and green indicating decreased expression, as indicated by the color intensity scale shown below each heatmap. Data in A–C were derived from three independent experiments and are presented as mean ± SD. *, $P < 0.05$ (*t* test).

Published OnlineFirst June 29, 2015; DOI: 10.1158/0008-5472.CAN-14-3265

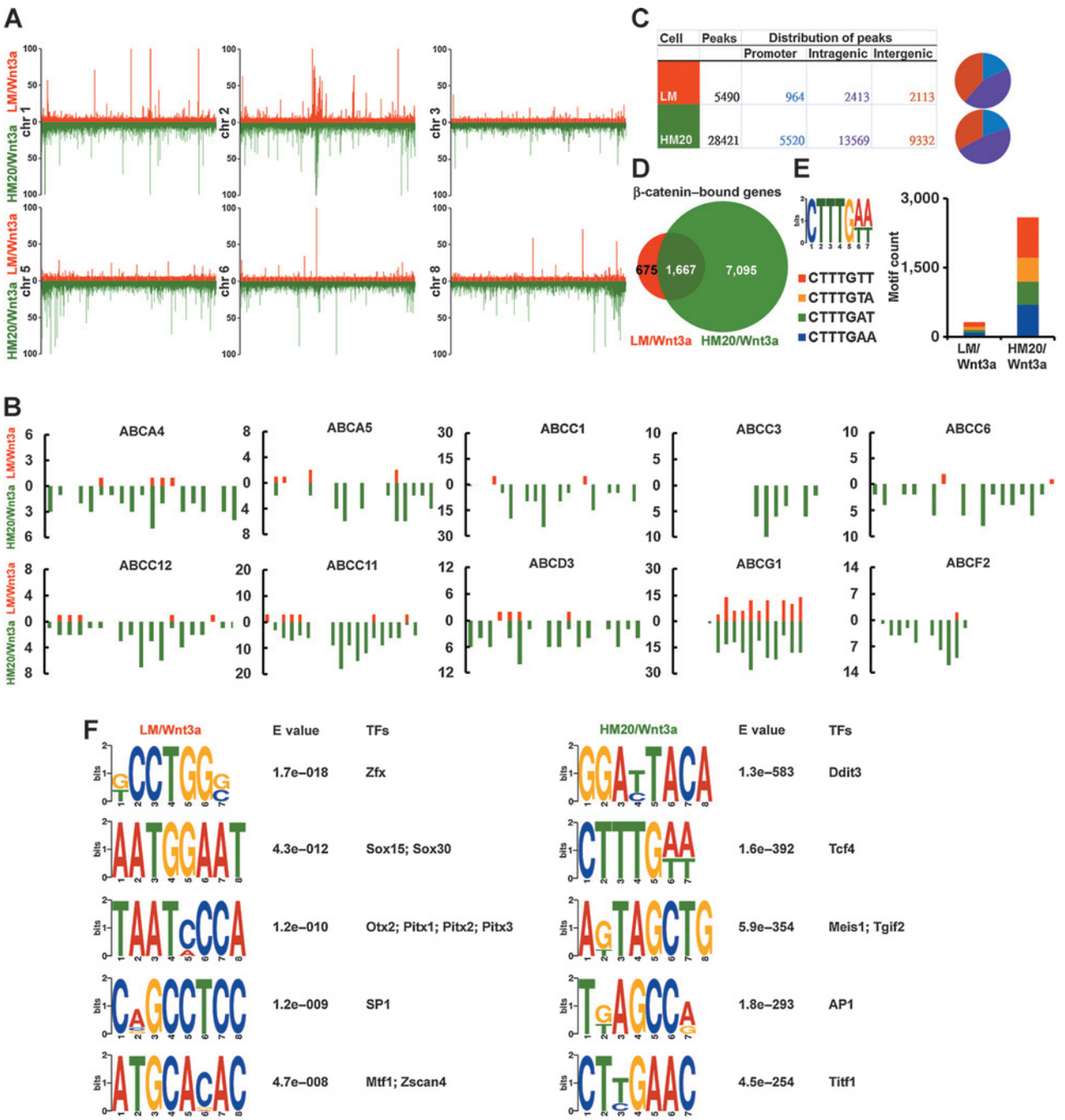

Figure 2.
Genome-wide mapping of β-catenin–binding sites in LM and HM20 cells after stimulation with Wnt3a. A and B, ChIP-seq profiles for binding of β-catenin complexes in LM (red) and HM20 (green) cells after stimulation with Wnt3a. Illustrative regions include chr 1 (10,020–249,240,417), chr 2 (150,646–242,962,001), chr 3 (154,704–197,866,845), chr 5 (12,995–180,707,461), chr 6 (172,769–170,871,342), and chr 8 (208,239–146,273,180) in A; ABCA4 (93,508,395–95,608,395), ABCA5 (66,290,575–68,390,575), ABCC1 (15,093,433–17,193,433), ABCC11 (47,250,821–49,350,821), ABCC12 (47,166,883–49,266,883), ABCC3 (47,762,217–49,862,217), ABCC6 (15,293,422–17,393,422), ABCD3 (93,933,932–96,033,932), ABCF2 (149,954,922–152,054,922), and ABCG1 (42,669,798–44,769,798) in B. C, ChIP-seq was used to map β-catenin complex binding in LM and HM20 cells after stimulation with Wnt3a. The distribution of β-catenin–binding sites was analyzed based on their location: promoter (from 10 kb upstream to the transcriptional start site), intragenic, and intergenic regions. D, Venn diagram showing the number of genes bound by the β-catenin complex in LM cells only, in HM20 cells only, and in both cell types after stimulation with Wnt3a. E, the number of TCF-binding motifs that were present in the peak sequences of LM and HM20 cells after Wnt3a treatment was scored. The numbers in the bar graph are the sum of each peak sequence (CTTTGAA, CTTTGAT, CTTTGTA, and CTTTGTT). F, a parallel version of MEME software was used to perform a *de novo* search of consensus binding motifs for β-catenin and transcription factors bound in LM and HM20 cells.

Published OnlineFirst June 29, 2015; DOI: 10.1158/0008-5472.CAN-14-3265

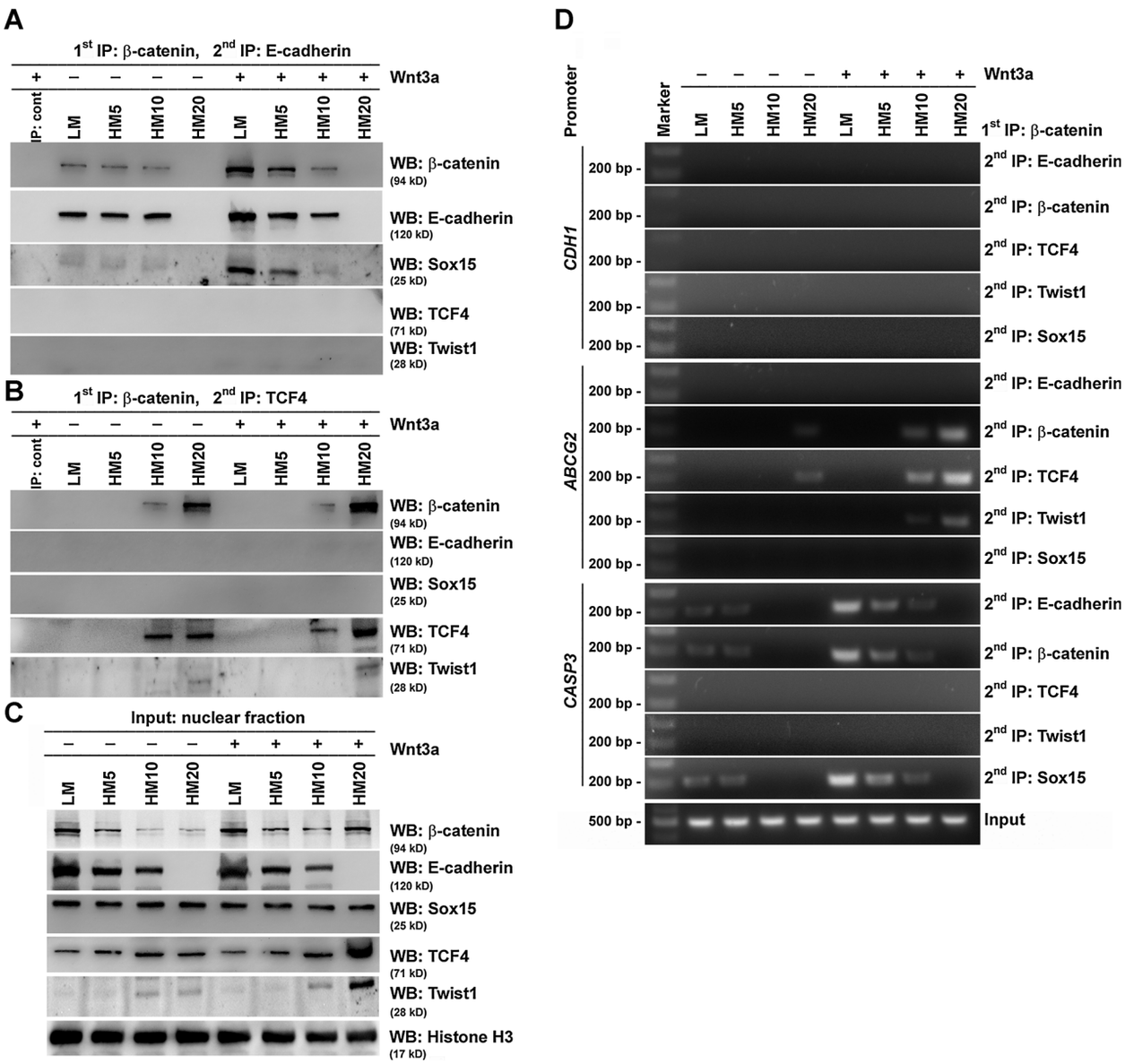

Figure 3.

EMT acts as a molecular switch from β-catenin/E-cadherin/Sox15 to β-catenin/Twist1/TCF4 complex formation. A–C, nuclear fractions were prepared from cells after subsequent serial selection (LM–HM20) with or without Wnt3a treatment. For tandem coimmunoprecipitation, nuclear fractions were immunoprecipitated with anti-β-catenin for the first precipitation, followed by a second immunoprecipitation of the first round–precipitated proteins with anti-E-cadherin (A) or anti-TCF4 (B). Proteins in the second immunoprecipitates were analyzed by Western blotting as indicated. D, nuclear extracts were prepared from cells as described in A. For re-ChIP, the DNA was immunoprecipitated with anti-β-catenin for the first precipitation, followed by a second immunoprecipitation after DNA isolation with antibodies against E-cadherin, β-catenin, TCF4, Twist1, or Sox15. Extracted DNA was analyzed by PCR using primers spanning the proximal promoter regions of *CDH1*, *ABCG2*, or *CASP3*.

multiple copies of wild-type TCF-binding sites) reporter activity (Fig. 4A) and the side population percentage (Fig. 4B) only in cells that expressed lower E-cadherin levels. However, Twist1 can promote Wnt/β-catenin–elicited transcriptional activity and the CSC phenotype (Wnt3a/Twist1; Fig. 4A and B). To gain more insight into the molecular mechanisms underlying tumor promotion by Twist1, we investigated associations of Twist1 with Wnt signaling–related molecules. Figure 4C shows that Twist1 associated with phospho-β-catenin (PS33,37/PT41). In addition, this association could be enhanced by Wnt3a stimulation, which was associated with an increase in TCF4 in Twist1 immunoprecipitates only from HM20 cells (Fig. 4D).

As noted above, the formation of the β-catenin/E-cadherin/Sox15 complex (which then bound to the proximal promoter region of *CASP3*) was enhanced by Wnt3a stimulation (Fig. 3). A recent study has demonstrated that Twist contains a putative caspase-3/7 consensus site (DELD) between amino acids (aa) 166 and 169 (7). Twist is a substrate for cleavage by caspase-3/7, and its cleavage results in ubiquitin-mediated proteasome degradation (7). Consistent with this observation, Wnt3a stimulation

Published OnlineFirst June 29, 2015; DOI: 10.1158/0008-5472.CAN-14-3265

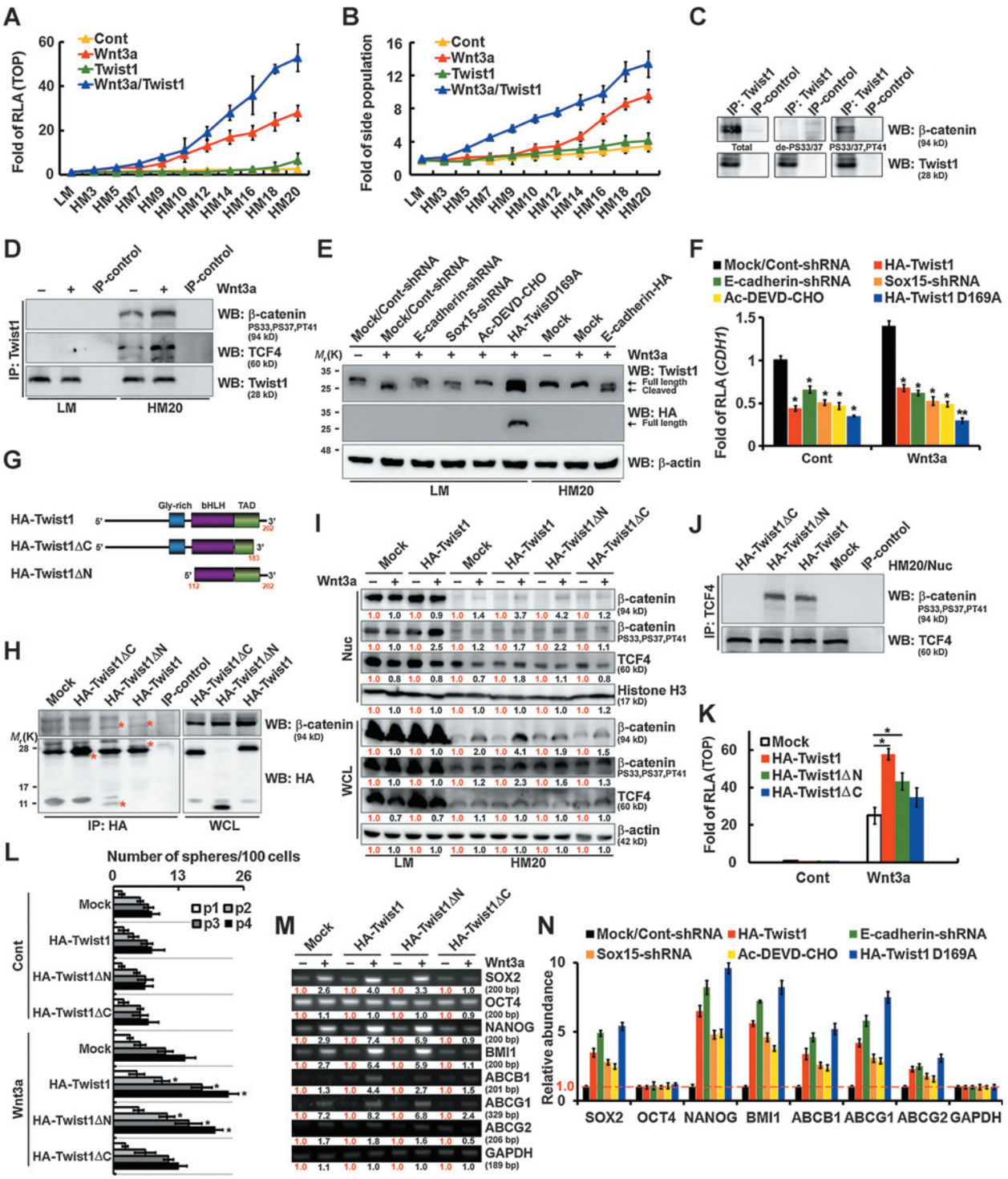

Figure 4.

β-Catenin/E-cadherin/Sox15 and β-catenin/Twist1/TCF4 possess opposing effects in regulating Wnt-elicited promotion of the CSC phenotype. A, whole-cell lysates were prepared from cells after subsequent serial selection (LM–HM20) and were transfected with either a plasmid encoding Twist1 or a control plasmid prior to treatment either with or without Wnt3a. A TOPflash luciferase reporter assay was then performed. B, cells selected as described in A were stained with Hoechst 33342 and side population cells were counted. C and D, whole-cell lysates (C) and nuclear fractions (D) were prepared from LM (D) and HM20 (C and D) cells and then immunoprecipitated using anti-Twist1 followed by Western blotting. E, whole-cell lysates were prepared from LM or HM20 cells infected with a lentivirus encoding an shRNA targeting E-cadherin or Sox15 or transfected with plasmids encoding E-cadherin or Twist1D169A prior to Wnt3a treatment followed by Western blotting. F, whole-cell lysates were prepared from LM cells as described in E. A luciferase reporter assay for *CDH1* promoter activity was then performed. (*Continued on the following page.*)

Published OnlineFirst June 29, 2015; DOI: 10.1158/0008-5472.CAN-14-3265

in LM cells and E-cadherin expression in HM20 cells triggered Twist1 cleavage, whereas Twist1D169A was not cleaved under the same conditions (Fig. 4E). Inhibition of caspase-dependent Twist cleavage by Ac-DEVD-CHO or by Sox15 or E-cadherin RNAi in LM cells abolished the effect on Twist1 cleavage (Fig. 4E). Similar results were shown in CL1-0 and CL1-5 cells (Supplementary Fig. S6A).

To measure the effect of E-cadherin/β-catenin/Sox15-mediated Twist1 cleavage, we determined *CDH1* (E-cadherin) promoter activity using luciferase reporter assays. After stimulation with Wnt3a, mock-transfected LM cells exhibited an increase in *CDH1* promoter activity compared with mock-transfected controls, suggesting that E-cadherin/β-catenin/Sox15 leads to increased *CDH1* promoter activity (abolishing Twist-mediated inhibition; Fig. 4F). Consistent with this observation, inhibition of the formation of E-cadherin/β-catenin/Sox15 complexes by E-cadherin or Sox15 RNAi abolished E-cadherin/Sox15–mediated enhancement in *CDH1* promoter activity (Fig. 4F). In addition, inhibition of caspase-dependent Twist cleavage by Ac-DEVD-CHO or the expression of Twist1D169A also decreased *CDH1* promoter activity (Fig. 4F)

To further define the effects of caspase-dependent Twist cleavage that are involved in association with β-catenin, deletion mutants were generated from the wild-type (Fig. 4G). Twist1ΔC (which mimics caspase-cleaved Twist1) failed to associate with β-catenin, indicating that the C-terminal domain (residues 184–202) of Twist1 is important for their association (Fig. 4H). β-Catenin–associating Twist1 may have contributed to β-catenin stabilization (Fig. 4I) by associating with phospho-β-catenin (Fig. 4J) and then enhancing Wnt3a-mediated β-catenin/TCF transcriptional activity in HM20 cells (Fig. 4K). When we characterized the effect of Twist1 on Wnt/β-catenin–elicited promotion of the CSC phenotype compared with controls, we found that β-catenin–associating Twist1 dramatically promoted the ability of cells to form spheres in culture over 4 serial passages (Fig. 4L). It also promoted the expression of stem cell–related and ABC transporter genes (Fig. 4M) after stimulation with Wnt3a whereas Twist1ΔC did not. Consistent with this observation, in LM cells compared with controls, inhibition of E-cadherin/β-catenin/Sox15 complex formation by E-cadherin or Sox15 RNAi and inhibition of caspase-dependent Twist cleavage by Ac-DEVD-CHO or expression of Twist1D169A substantially promoted the expression of stem cell–related and ABC transporter genes after stimulation with Wnt3a (Fig. 4N). Similar results were shown in CL1-0 and CL1-5 cells (Supplementary Fig. S6B–S6D).

Canonical Wnt signaling is required for an EMT-driven gain of CSC properties in experimental animal models

For *in vivo* tumorigenicity assays, mice were injected subcutaneously with 10^4 to 10^2 cells. In a dose–response experiment on LM and HM20 cells (10^3–10^4 cells) with or without Wnt3a treatment injected per mouse, no differences in the tumorigenic potential (Fig. 5A and B) or tumor growth (Fig. 5C and D) were evident unless 10^2 cells (only in HM20 cells; Fig. 5A, B, and E) were injected. LM cells transfected with E-cadherin or Sox15 shRNA or with a Twist1/D169A vector after Wnt3a treatment showed the highest tumorigenic potential and more tumor growth when injected with as few as 10^2 cells (Fig. 5A and E). In addition, Twist1 expression in HM20 cells (10^2 cells) further enhanced the Wnt3a-elicited tumorigenic potential (Fig. 5B) and tumor growth (Fig. 5E), whereas E-cadherin expression significantly disrupted Wnt3a-elicited functions (Fig. 5B). To test whether cancer cells derived from xenografts (described in Fig. 5E) exhibited the properties of CSCs and an EMT phenotype, the resultant tumors were analyzed. The pattern of CSC-related gene (ABCG2 and CD133) expression in the secondary tumors *in vivo* was significantly higher, whereas E-cadherin was significantly lower, compared with *in vitro* observations (Fig. 5F and Supplementary Fig. S7).

Five-gene signature (nuclear β-catenin^{High}/nuclear Twist1^{High}/E-cadherin^{Low}/Sox15^{Low}/CD133^{High}) is closely associated with progression and metastasis in patients with lung cancer

To validate the clinical relevance of the EMT/Wnt/β-catenin pathway to human cancer and its contribution to promotion of the CSC phenotype during lung tumorigenesis, we analyzed the expression profiles of nuclear β-catenin, nuclear Twist1, E-cadherin, Sox15, and CD133. We used IHC staining and scoring (8, 26) in consecutive slides from 108 primary (stages IA, IB, IIA, IIB, III, and IV) and 10 metastatic human lung cancer specimens. Low-grade (stages IA and IB) primary lung cancers showed low levels of nuclear β-catenin, nuclear Twist1, and CD133 and high levels of E-cadherin and Sox15 (Fig. 6A). In contrast, high-grade (stages III and IV) primary and metastatic lung cancers showed high levels of nuclear β-catenin, nuclear Twist1, and CD133 and low levels of E-cadherin and Sox15 (Fig. 6A). Notably, we observed a direct association between tumor grade and the nuclear β-catenin, nuclear Twist1, and CD133 signals. These reached their maximum in high-grade (stages III and IV) primary and metastatic lung cancers, whereas E-cadherin and Sox15 signals reached their maximum in low-grade (stages IA and IB) primary lung cancers (Fig. 6B–G).

Using a bimodal IHC score distribution, tissues with IHC scores that were lower than average were designated as having "Low" expression, and scores that were higher than average were designated as having "High" expression (designations shown in Fig. 6G; e.g., nuclear Twist1^{H}). The percentage of patients displaying the pattern signature of nuclear β-catenin^{High}, nuclear Twist1^{High}, E-cadherin^{Low}, Sox15^{Low}, and CD133^{High} expression (which

(*Continued.*) G, schematic representation of HA-tagged wild-type, C-terminal deletion (Twist1ΔC), and N-terminal deletion (Twist1ΔN) Twist1 proteins. H, whole-cell lysates were prepared from HM20 cells transfected with plasmids encoding wild-type Twist1, Twist1ΔC, or Twist1ΔN after treatment in the absence or presence of Wnt3a, and then proteins were immunoprecipitated using anti-HA followed by Western blotting. Asterisks indicate the target proteins with expected sizes. I, Western blot analysis of the nuclear fraction and whole-cell lysates of LM and HM20 cells as described in H was performed. The relative intensities of the bands are shown. J, nuclear fraction was prepared from HM20 cells as described in H, and then proteins were immunoprecipitated using anti-TCF4 followed by Western blotting. Asterisks indicate the target proteins with expected sizes. K, whole-cell lysates were prepared from HM20 cells as described in H. A TOPflash luciferase reporter assay was performed. L, quantification of spheres formed by HM20 cells as described in H for four serial passages (p1–p4). The individual spheres were found to be derived from single cells. M, mRNA was prepared from HM20 cells as described in H. The expression of stem cell–related and ABC transporter genes was evaluated by RT-PCR. The relative intensities of the bands are shown. N, mRNA was prepared from LM cells as described in E. The expression of stem cell–related and ABC transporter genes was evaluated by RT-PCR and compared with cells treated with control medium. Data in A, B, F, K, L, and N were derived from three independent experiments and are presented as mean ± SD. *, $P < 0.05$; **, $P < 0.01$ (*t* test). RLA, relative luciferase activity.

Published OnlineFirst June 29, 2015; DOI: 10.1158/0008-5472.CAN-14-3265

A

			Tumorigenesis (SC)		
			10^4 cells	10^3 cells	10^2 cells
LM	Cont	Mock	5/5	5/5	0/6
	Wnt3a	Mock	5/5	3/5	0/6
		E-cad-shRNA		5/5	6/6
		Sox15-shRNA		5/5	6/6
		Twist1/D169A		5/5	6/6

B

			Tumorigenesis (SC)		
			10^4 cells	10^3 cells	10^2 cells
HM20	Cont	Mock	5/5	5/5	2/6
	Wnt3a	Mock	5/5	5/5	4/6
		E-cad		5/5	0/6
		Twist1		5/5	6/6

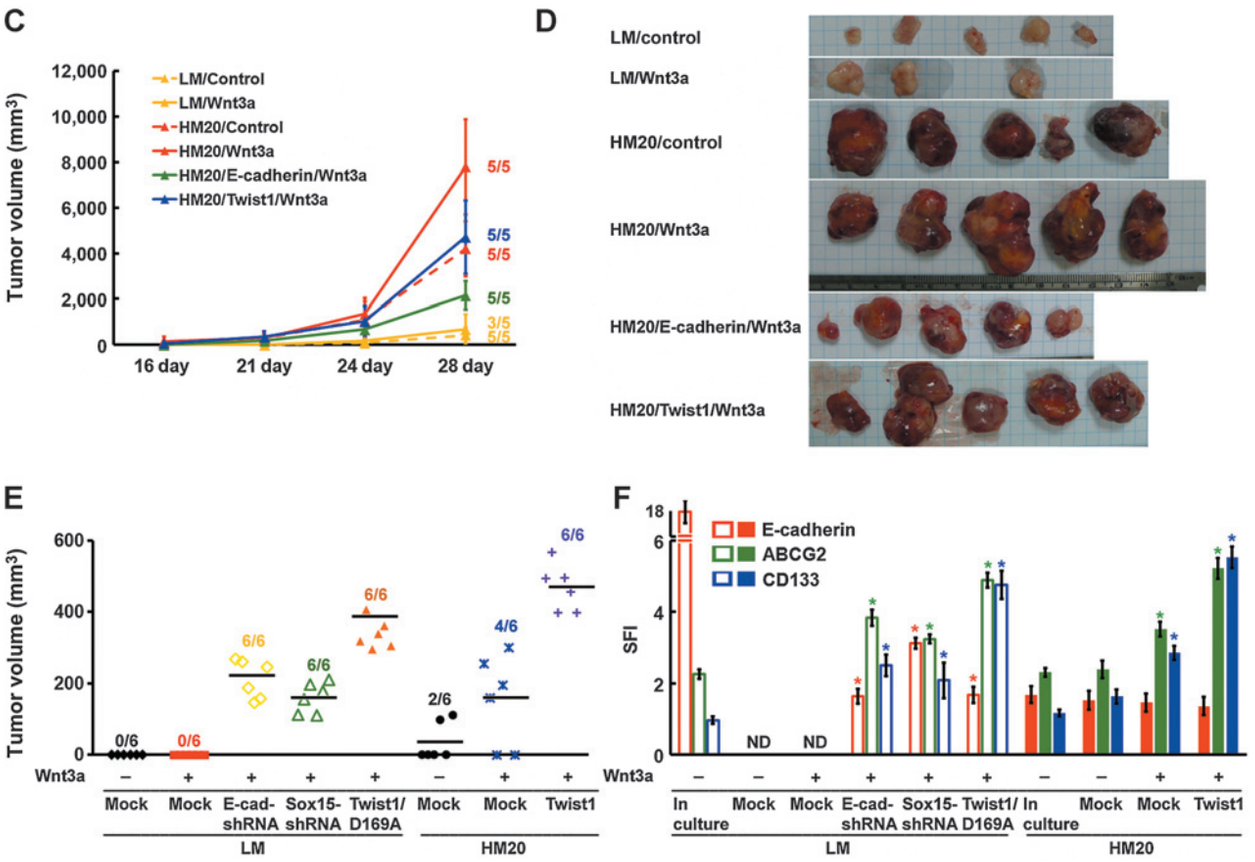

Figure 5.
Canonical Wnt signaling is required for an EMT-driven gain of CSC properties in experimental animal models. A and B, for *in vivo* tumorigenicity assay, mice were injected subcutaneously with 10^2 to 10^4 LM (A) or HM20 (B) cells in 100 μL of a 1:1 mixture of DMEM (with control medium or Wnt3a)/Matrigel. Mice were euthanized at 28 days after transplantation. E-cad, E-cadherin. C and D, for *in vivo* tumorigenicity assay as described in A and B, tumor volumes were evaluated at 16, 21, 24, and 28 days after transplantation in mice injected subcutaneously with 10^3 cells. Representative images of tumors (mice euthanized at 28 days) generated are shown in D. E, for *in vivo* tumorigenicity assay as described in A and B, tumor volumes were evaluated at 28 days after transplantation in mice injected subcutaneously with 10^2 cells. F, cancer cells derived from the xenografts as described in E were analyzed. The level of E-cadherin, ABCG2, and CD133 expression was determined by flow cytometry. The specific fluorescence index was calculated as the ratio of the geometric mean fluorescence value obtained with the specific antibody and the isotype control antibody. Data in D were derived from three independent experiments and are presented as mean ± SD. *, $P < 0.05$ (*t* test).

suggests hyperactivity of the EMT/Wnt/β-catenin pathway) increased in line with the increase in tumor grade (Fig. 6G). These results further support the idea that the 5-gene signature (nuclear β-catenin^{High}/nuclear Twist1^{High}/E-cadherin^{Low}/Sox15^{Low}/CD133^{High}) is closely associated with progression and metastasis in patients with lung cancer and indicates that these proteins could serve as predictors for poor overall patient survival.

Discussion

Several reports suggest that EMT generates cancer cells with stem cell–like properties in various cancers, including lung cancer (27). Few studies have focused on illustrating the detailed molecular mechanism that links EMT and stemness. However, some of the paracrine/autocrine signaling necessary for stem cell–like properties was recently shown to be induced through EMT (2).

Published OnlineFirst June 29, 2015; DOI: 10.1158/0008-5472.CAN-14-3265

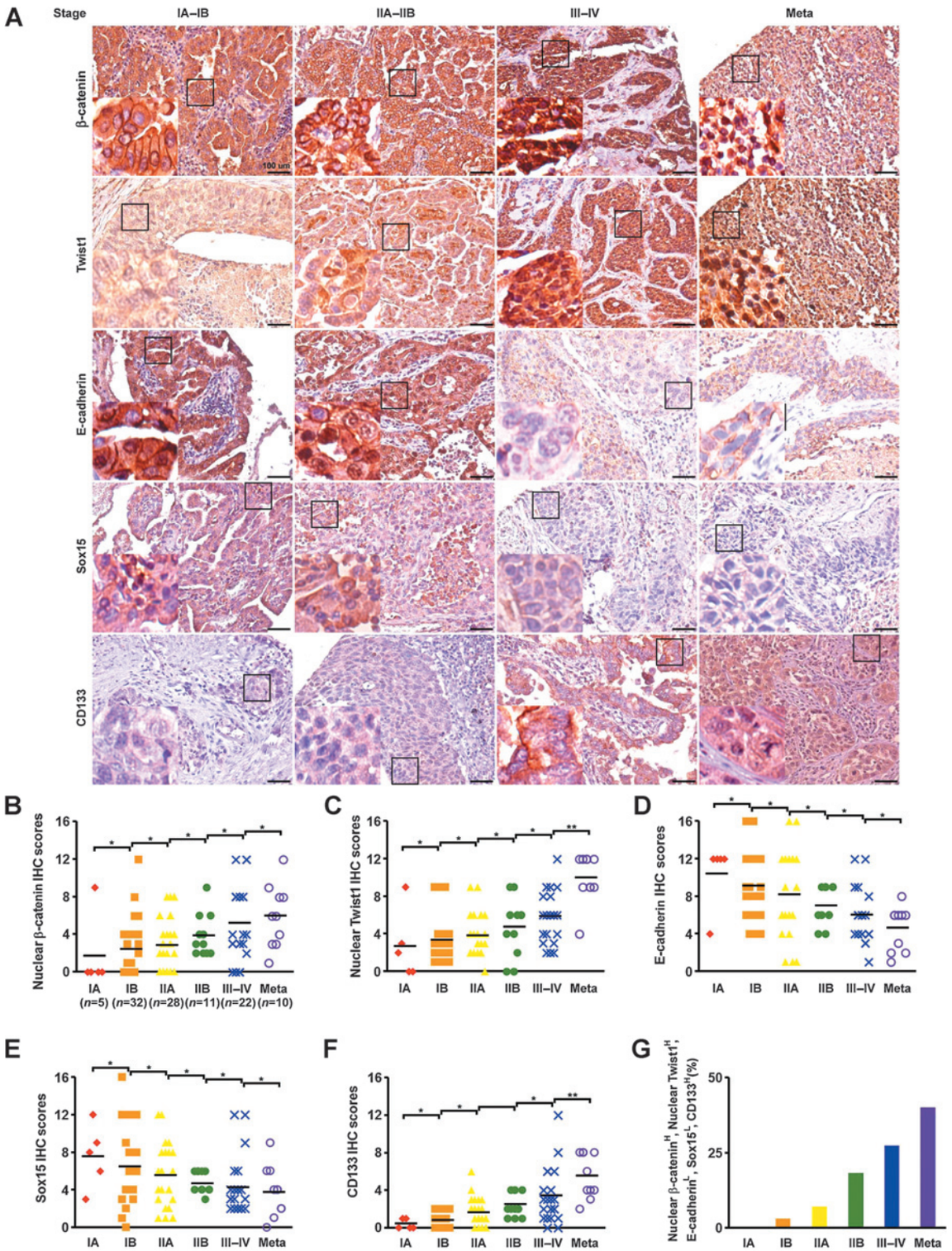

Figure 6.
Clinical significance of β-catenin, Twist1, E-cadherin, Sox15, and CD133 in patients with lung cancer. A, immunohistochemistry for β-catenin, Twist1, E-cadherin, Sox15, and CD133 in representative tumor tissues from patients with lung cancer. Both primary and metastatic (Meta) cancer specimens are shown. Only nuclear positivity of β-catenin and Twist1 was considered significant. Staging of the primary cancers was carried out according to AJCC Cancer Staging Manual (7th edition). Tissues were counterstained with hematoxylin. Left bottom, enlarged images from boxed areas as indicated. Bars, 100 μm. B–F, quantification of nuclear β-catenin (B), nuclear Twist1 (C), E-cadherin (D), Sox15 (E), and CD133 (F) expression (i.e., IHC scores) during lung tumorigenesis. Total number of cases in each group is indicated at the bottom. Black bars, the average score within each group of specimens. *, $P < 0.05$; **, $P < 0.01$. G, percentage of patients displaying the signature expression pattern of nuclear β-catenin^{High}, nuclear Twist1^{High}, E-cadherin^{Low}, Sox15^{Low}, and CD133^{High} in different stages of primary and metastatic lung cancers.

Published OnlineFirst June 29, 2015; DOI: 10.1158/0008-5472.CAN-14-3265

Here, we demonstrate a convergence of factors from 2 different mechanisms—EMT and the canonical Wnt signaling pathway. It is still not known whether an active signaling pathway can successfully operate reprogramming in mesenchymal-type, rather than epithelial-type, cancer cells. Many results support a model in which β-catenin provides a platform for the recruitment of a multitude of transcriptional co-activators initiating or modifying Wnt/β-catenin transcription. ChIP-based time course experiments focusing on β-catenin target promoters support a dynamic cycling mechanism (28). It is likely that there will be cell and gene-specific mechanisms as well. We found in this study that in epithelial cells, Sox15 functioned as a repressor of EMT by interacting with β-catenin in Wnt/β-catenin signaling. In mesenchymal cells, Twist1 associated with β-catenin and enhanced β-catenin/TCF transcriptional activity (Supplementary Fig. S8).

In parallel, binding of Wnt to Frizzled receptor leads to hyperphosphorylation of the Disheveled protein (29), which, through its association with the destruction complex [consisting of the scaffold proteins Axin (30) and adenoma polyposis coli (APC; ref. 31), and of the kinases phosphorylating β-catenin, GSK3β (32), casein kinase 1 (CK1), and protein phosphatase 2A (PP2A; ref. 33)] prevents the complex from phosphorylating β-catenin (34). Unphosphorylated β-catenin is stabilized by escaping recognition by β-TrCP (35), a component of an E3 ubiquitin ligase, and it eventually translocates into the nucleus, where it binds to the transcription factors LEF/TCF (36) to activate expression of downstream genes. APC binds to the armadillo repeat regions of β-catenin, which are the same binding sites as for E-cadherin; hence, the interactions of β-catenin with APC and E-cadherin are mutually exclusive (37). In our study, we found that in epithelial-type cells β-catenin associated with E-cadherin, preventing APC (the destruction complex) from binding to β-catenin as anticipated. In addition, the binding sites on β-catenin for TCF4 and E-cadherins are also mutually exclusive, and overexpression of E-cadherin can block TCF4/β-catenin–mediated transcription *in vitro* (38). Consistent with these findings, we demonstrated that Sox15 (instead of TCF4), in complex with β-catenin and E-cadherin (Fig. 3A), bound to the proximal promoter region of *CASP3* (not a putative TCF4/β-catenin target gene).

The mechanisms by which Wnt inhibits the destruction complex are only partially understood, but recent work has indicated that a key step regulated by Wnt is the dissociation of β-TrCP from the complex (39). β-Catenin is presented to the proteasome through its interaction with the F-box–containing E3 ligase protein β-TrCP, an adaptor protein that forms a complex with the Skp1/Cullin machinery to attach ubiquitin to its binding partners (35). The binding site for β-TrCP on β-catenin is a short peptide that encompasses 2 conserved serines, Ser33 and Ser37, which when phosphorylated, interact with the β-propeller domain of β-TrCP (40). In our data, Twist1 contributed to β-catenin stabilization in mesenchymal cells (Fig. 4I) by associating with phospho-β-catenin (phosphorylated at Ser33/37; Fig. 4C) and then enhancing Wnt3a-mediated β-catenin/TCF transcriptional activity in HM20 cells (Fig. 4K). Twist1/β-Catenin association did not interfere with β-catenin binding to the destruction complex because Ser33 and Ser37 of β-catenin could still be phosphorylated. However, the interactions of phospho-β-catenin with Twist1 and β-TrCP are mutually exclusive. Phospho-β-catenin association with Twist1 prevented it from binding to β-TrCP. Consequently, β-catenin was stabilized by escaping recognition by β-TrCP and eventually translocated to the nucleus where it engaged the transcription factors LEF/TCF4 to activate expression of downstream genes.

Unexpectedly, not all β-catenin phosphorylated by GSK3β undergoes degradation. A fraction of phospho-β-catenin (phosphorylated at Ser33/37) is detected in centrosomes, which contributes to centrosomal cohesion and separation at the onset of mitotic spindle formation (41). Phospho-β-catenin localizes to the centrosomes of neuronal progenitors and is required for cell polarity and neurogenesis in the developing midbrain (42). Although phospho-β-catenin has a short half-life, degradation of phospho-β-catenin appears to be determined by its subcellular localization (43). It is likely that β-catenin is phosphorylated by GSK3β in the nucleus, where it is protected from degradation, allowing it to accumulate until mitosis, and it is then released to the cytoplasm when the nuclear membrane is broken (41). In G_2–M, nuclear accumulation of phospho-β-catenin protects it from degradation. In contrast, phospho-β-catenin released to the cytoplasm is rapidly degraded when cells enter into the next G_1 phase (41). Here, we found that Twist1 associated with phospho-β-catenin (PS33,37/PT41; Fig. 4C) and prevented it from being released to the cytosol (increased nuclear phospho-β-catenin; Fig. 4I).

Caspase-mediated cleavage may result in either substrate activation or in protein inactivation. We have shown that caspase-mediated proteolysis results in Twist inactivation, consistent with results of a previous study (7), which demonstrated that the DELD motif at positions 166 to 169 of the Twist protein was recognized as a cleavage site by caspase-3. Although the critical function of caspase-3 in apoptosis is firmly established, an increasing number of studies have unexpectedly revealed various nonapoptotic functions of caspase-3, including mediating lymphocyte proliferation, erythroblasts, lens epithelial cells, skeletal muscle cells, neural differentiation, and stem cell maintenance (44, 45). A nonapoptotic role for caspase-3 in the regulation of cell proliferation (45) and differentiation (44) is suggested by its ability to cleave substrates associated with cell-cycle control (p21; ref. 45) and to finely modulate differentiation (Nanog; ref. 44). It will be of great interest to test the regulation of caspase-3 activation under nonapoptotic conditions. The time is ripe for further exploration of the nonapoptotic functions of caspases-3 and for the systematic identification of caspase-3 substrates that might function as critical effectors for these cellular processes.

Accumulating clinical evidence has demonstrated that E-cadherin (17), β-catenin (46), and Twist1 (47) are markers of malignancy for different cancers, whereas their functional relationships have not been completely delineated. To confirm that the cooperative role between β-catenin and Twist1 occurs across multiple cancers, we tested tumor samples from patients with lung cancer. SOX family members, such as *SOX17* (48) and *SOX6* (49), are established tumor suppressor genes in other cancer types, whereas *SOX15* has not previously been described as a tumor suppressor gene. We found that Sox15 associated with the β-catenin/E-cadherin complex and then bound to the proximal promoter regions of *CASP3*, consequently resulting in Twist1 cleavage in epithelial-type cells. Sox15 could thus act as a negative regulator of Wnt signaling–elicited promotion of the CSC phenotype. Furthermore, compared with low-grade cancer, both high-grade and metastatic cancer exhibited markedly downregulated Sox15 in clinical human lung cancer specimens. This observation implies that the combination of nuclear β-catenin^{High}/nuclear Twist1^{High}/E-cadherin^{Low}/Sox15^{Low}/CD133^{High} may be

regarded as predictive for poorer outcomes of patients with lung cancer.

Disclosure of Potential Conflicts of Interest

No potential conflicts of interest were disclosed.

Authors' Contributions

Conception and design: Y.-W. Chang, Y.-J. Su, S.-C. Chen, J.-L. Lee
Development of methodology: W.-H. Lin, C.-J. Liang, S.-C. Chen
Acquisition of data (provided animals, acquired and managed patients, provided facilities, etc.): K.-C. Wei, S.-C. Chen
Analysis and interpretation of data (e.g., statistical analysis, biostatistics, computational analysis): Y.-W. Chang, Y.-J. Su, S.-C. Chen, J.-L. Lee
Writing, review, and/or revision of the manuscript: Y.-W. Chang, Y.-J. Su, S.-C. Chen, J.-L. Lee
Administrative, technical, or material support (i.e., reporting or organizing data, constructing databases): M. Hsiao, K.-C. Wei, W.-H. Lin, S.-C. Chen

Acknowledgments

The authors thank Margaret Dah-Tsyr Chang for comments on this article. They acknowledge access to the Biomedical Science and Engineering Center, National Tsing Hua University (Hsinchu, Taiwan) and thank Wen-Ching Wang for technical advice using the FACSAria III (BD Biosciences) flow cytometer.

Grant Support

This work was supported by funds from the Ministry of Science and Technology, Taiwan Grant 103-2314-B-007-001, and the National Health Research Institutes, Taiwan Grant NHRI-EX101-10018BC.

The costs of publication of this article were defrayed in part by the payment of page charges. This article must therefore be hereby marked *advertisement* in accordance with 18 U.S.C. Section 1734 solely to indicate this fact.

Received November 11, 2014; revised April 22, 2015; accepted May 13, 2015; published OnlineFirst June 29, 2015.

References

1. Mani SA, Guo W, Liao MJ, Eaton EN, Ayyanan A, Zhou AY, et al. The epithelial-mesenchymal transition generates cells with properties of stem cells. Cell 2008;133:704–15.
2. Scheel C, Eaton EN, Li SH, Chaffer CL, Reinhardt F, Kah KJ, et al. Paracrine and autocrine signals induce and maintain mesenchymal and stem cell states in the breast. Cell 2011;145:926–40.
3. Thiery JP, Sleeman JP. Complex networks orchestrate epithelial-mesenchymal transitions. Nat Rev Mol Cell Biol 2006;7:131–42.
4. Yang MH, Hsu DS, Wang HW, Wang HJ, Lan HY, Yang WH, et al. Bmi1 is essential in Twist1-induced epithelial-mesenchymal transition. Nat Cell Biol 2010;12:982–92.
5. Chung MT, Lai HC, Sytwu HK, Yan MD, Shih YL, Chang CC, et al. SFRP1 and SFRP2 suppress the transformation and invasion abilities of cervical cancer cells through Wnt signal pathway. Gynecol Oncol 2009;112:646–53.
6. Shiota M, Izumi H, Tanimoto A, Takahashi M, Miyamoto N, Kashiwagi E, et al. Programmed cell death protein 4 down-regulates Y-box binding protein-1 expression via a direct interaction with Twist1 to suppress cancer cell growth. Cancer Res 2009;69:3148–56.
7. Demontis S, Rigo C, Piccinin S, Mizzau M, Sonego M, Fabris M, et al. Twist is substrate for caspase cleavage and proteasome-mediated degradation. Cell Death Differ 2006;13:335–45.
8. Lee JL, Chang CJ, Wu SY, Sargan DR, Lin CT. Secreted frizzled-related protein 2 (SFRP2) is highly expressed in canine mammary gland tumors but not in normal mammary glands. Breast Cancer Res Treat 2004;84:139–49.
9. Su YJ, Lai HM, Chang YW, Chen GY, Lee JL. Direct reprogramming of stem cell properties in colon cancer cells by CD44. EMBO J 2011;30:3186–99.
10. Li H, Durbin R. Fast and accurate short read alignment with Burrows-Wheeler transform. Bioinformatics 2009;25:1754–60.
11. Bailey TL, Elkan C. Fitting a mixture model by expectation maximization to discover motifs in biopolymers. Proc Int Conf Intell Syst Mol Biol 1994;2:28–36.
12. Machanick P, Bailey TL. MEME-ChIP: motif analysis of large DNA datasets. Bioinformatics 2011;27:1696–7.
13. Bardet AF, He Q, Zeitlinger J, Stark A. A computational pipeline for comparative ChIP-seq analyses. Nat Protoc 2012;7:45–61.
14. Portales-Casamar E, Thongjuea S, Kwon AT, Arenillas D, Zhao X, Valen E, et al. JASPAR 2010: the greatly expanded open-access database of transcription factor binding profiles. Nucleic Acids Res 2010;38:D105–10.
15. Robasky K, Bulyk ML. UniPROBE, update 2011: expanded content and search tools in the online database of protein-binding microarray data on protein-DNA interactions. Nucleic Acids Res 2011;39:D124–8.
16. Lee JL, Wang MJ, Chen JY. Acetylation and activation of STAT3 mediated by nuclear translocation of CD44. J Cell Biol 2009;185:949–57.
17. Chen XF, Zhang HT, Qi QY, Sun MM, Tao LY. Expression of E-cadherin and nm23 is associated with the clinicopathological factors of human non-small cell lung cancer in China. Lung Cancer 2005;48:69–76.
18. Lee JL, Lin CT, Chueh LL, Chang CJ. Autocrine/paracrine secreted Frizzled-related protein 2 induces cellular resistance to apoptosis: a possible mechanism of mammary tumorigenesis. J Biol Chem 2004;279:14602–9.
19. Miettinen PJ, Ebner R, Lopez AR, Derynck R. TGF-beta induced transdifferentiation of mammary epithelial cells to mesenchymal cells: involvement of type I receptors. J Cell Biol 1994;127:2021–36.
20. Wu Y, Ginther C, Kim J, Mosher N, Chung S, Slamon D, et al. Expression of Wnt3 activates Wnt/beta-catenin pathway and promotes EMT-like phenotype in trastuzumab-resistant HER2-overexpressing breast cancer cells. Mol Cancer Res 2012;10:1597–606.
21. Kanzawa M, Semba S, Hara S, Itoh T, Yokozaki H. WNT5A is a key regulator of the epithelial-mesenchymal transition and cancer stem cell properties in human gastric carcinoma cells. Pathobiology 2013;80:235–44.
22. Hamada S, Satoh K, Hirota M, Kimura K, Kanno A, Masamune A, et al. Bone morphogenetic protein 4 induces epithelial-mesenchymal transition through MSX2 induction on pancreatic cancer cell line. J Cell Physiol 2007;213:768–74.
23. Chikazawa N, Tanaka H, Tasaka T, Nakamura M, Tanaka M, Onishi H, et al. Inhibition of Wnt signaling pathway decreases chemotherapy-resistant side-population colon cancer cells. Anticancer Res 2010;30:2041–8.
24. van de Wetering M, Oosterwegel M, Dooijes D, Clevers H. Identification and cloning of TCF-1, a T lymphocyte-specific transcription factor containing a sequence-specific HMG box. EMBO J 1991;10:123–32.
25. Chu YW, Yang PC, Yang SC, Shyu YC, Hendrix MJ, Wu R, et al. Selection of invasive and metastatic subpopulations from a human lung adenocarcinoma cell line. Am J Respir Cell Mol Biol 1997;17:353–60.
26. Camp RL, Rimm EB, Rimm DL. Met expression is associated with poor outcome in patients with axillary lymph node negative breast carcinoma. Cancer 1999;86:2259–65.
27. Pirozzi G, Tirino V, Camerlingo R, Franco R, La Rocca A, Liguori E, et al. Epithelial to mesenchymal transition by TGFbeta-1 induction increases stemness characteristics in primary non small cell lung cancer cell line. PLoS One 2011;6:e21548.
28. Sierra J, Yoshida T, Joazeiro CA, Jones KA. The APC tumor suppressor counteracts beta-catenin activation and H3K4 methylation at Wnt target genes. Genes Dev 2006;20:586–600.
29. Noordermeer J, Klingensmith J, Perrimon N, Nusse R. dishevelled and armadillo act in the wingless signalling pathway in Drosophila. Nature 1994;367:80–3.
30. Zeng L, Fagotto F, Zhang T, Hsu W, Vasicek TJ, Perry WL III, et al. The mouse Fused locus encodes Axin, an inhibitor of the Wnt signaling pathway that regulates embryonic axis formation. Cell 1997;90:181–92.
31. Groden J, Thliveris A, Samowitz W, Carlson M, Gelbert L, Albertsen H, et al. Identification and characterization of the familial adenomatous polyposis coli gene. Cell 1991;66:589–600.
32. He X, Saint-Jeannet JP, Woodgett JR, Varmus HE, Dawid IB. Glycogen synthase kinase-3 and dorsoventral patterning in Xenopus embryos. Nature 1995;374:617–22.

Published OnlineFirst June 29, 2015; DOI: 10.1158/0008-5472.CAN-14-3265

33. Kimelman D, Xu W. beta-catenin destruction complex: insights and questions from a structural perspective. Oncogene 2006;25:7482–91.
34. Spiegelman VS, Slaga TJ, Pagano M, Minamoto T, Ronai Z, Fuchs SY. Wnt/beta-catenin signaling induces the expression and activity of betaTrCP ubiquitin ligase receptor. Mol Cell 2000;5:877–82.
35. Hart M, Concordet JP, Lassot I, Albert I, del los Santos R, Durand H, et al. The F-box protein beta-TrCP associates with phosphorylated beta-catenin and regulates its activity in the cell. Curr Biol 1999;9:207–10.
36. Molenaar M, van de Wetering M, Oosterwegel M, Peterson-Maduro J, Godsave S, Korinek V, et al. XTcf-3 transcription factor mediates beta-catenin-induced axis formation in Xenopus embryos. Cell 1996;86:391–9.
37. Morin PJ. beta-catenin signaling and cancer. Bioessays 1999;21:1021–30.
38. Seidensticker MJ, Behrens J. Biochemical interactions in the wnt pathway. Biochim Biophys Acta 2000;1495:168–82.
39. Li VS, Ng SS, Boersema PJ, Low TY, Karthaus WR, Gerlach JP, et al. Wnt signaling through inhibition of beta-catenin degradation in an intact Axin1 complex. Cell 2012;149:1245–56.
40. Orford K, Crockett C, Jensen JP, Weissman AM, Byers SW. Serine phosphorylation-regulated ubiquitination and degradation of beta-catenin. J Biol Chem 1997;272:24735–8.
41. Huang P, Senga T, Hamaguchi M. A novel role of phospho-beta-catenin in microtubule regrowth at centrosome. Oncogene 2007;26:4357–71.
42. Chilov D, Sinjushina N, Rita H, Taketo MM, Makela TP, Partanen J. Phosphorylated beta-catenin localizes to centrosomes of neuronal progenitors and is required for cell polarity and neurogenesis in developing midbrain. Dev Biol 2011;357:259–68.
43. Sadot E, Conacci-Sorrell M, Zhurinsky J, Shnizer D, Lando Z, Zharhary D, et al. Regulation of S33/S37 phosphorylated beta-catenin in normal and transformed cells. J Cell Sci 2002;115:2771–80.
44. Fujita J, Crane AM, Souza MK, Dejosez M, Kyba M, Flavell RA, et al. Caspase activity mediates the differentiation of embryonic stem cells. Cell Stem Cell 2008;2:595–601.
45. Levkau B, Koyama H, Raines EW, Clurman BE, Herren B, Orth K, et al. Cleavage of p21Cip1/Waf1 and p27Kip1 mediates apoptosis in endothelial cells through activation of Cdk2: role of a caspase cascade. Mol Cell 1998;1:553–63.
46. Liu L, Zhu XD, Wang WQ, Shen Y, Qin Y, Ren ZG, et al. Activation of beta-catenin by hypoxia in hepatocellular carcinoma contributes to enhanced metastatic potential and poor prognosis. Clin Cancer Res 2010;16:2740–50.
47. Gomez I, Pena C, Herrera M, Munoz C, Larriba MJ, Garcia V, et al. TWIST1 is expressed in colorectal carcinomas and predicts patient survival. PLoS One 2011;6:e18023.
48. Du YC, Oshima H, Oguma K, Kitamura T, Itadani H, Fujimura T, et al. Induction and down-regulation of Sox17 and its possible roles during the course of gastrointestinal tumorigenesis. Gastroenterology 2009;137:1346–57.
49. Qin YR, Tang H, Xie F, Liu H, Zhu Y, Ai J, et al. Characterization of tumor-suppressive function of SOX6 in human esophageal squamous cell carcinoma. Clin Cancer Res 2011;17:46–55.

Cancer Research

Correction: Diverse Targets of β-Catenin during the Epithelial–Mesenchymal Transition Define Cancer Stem Cells and Predict Disease Relapse

In this article (Cancer Res 2015;75:3398–410), which appeared in the August 15, 2015, issue of *Cancer Research* (1), the correct name of the sixth author is Chi-Jung Liang.

The online version of the article has been corrected and no longer matches the print.

Reference

1. Chang Y-W, Su Y-J, Hsiao M, Wei K-C, Lin W-H, Liang C-J, et al. Diverse targets of β-catenin during the epithelial–mesenchymal transition define cancer stem cells and predict disease relapse. Cancer Res 2015;75:3398–410.

Published online October 14, 2016.
doi: 10.1158/0008-5472.CAN-16-2415

Published OnlineFirst June 29, 2015; DOI: 10.1158/0008-5472.CAN-14-3265

Cancer Research
The Journal of Cancer Research (1916–1930) | The American Journal of Cancer (1931–1940)

AACR American Association for Cancer Research

Diverse Targets of β-Catenin during the Epithelial–Mesenchymal Transition Define Cancer Stem Cells and Predict Disease Relapse

Yi-Wen Chang, Ying-Jhen Su, Michael Hsiao, et al.

Cancer Res 2015;75:3398-3410. Published OnlineFirst June 29, 2015.